International Journal of Thermophysics, Vol. 22, No. 1, 2001

Impact of Experimental Timescale and Geometry on Thin-Film Thermal Property Measurements[1]

M. N. Touzelbaev[2] and K. E. Goodson[2, 3]

Integrated circuits require effective removal of increasing heat fluxes from active regions. Thermal conduction strongly influences the performance of micromachined devices including thermal actuators, Peltier-effect coolers, and bolometers. The simulation of these devices requires thermal property data for the thin-film materials from which they are made. While there are many measurement techniques available, it is often difficult to identify the most appropriate for a device. This article reviews thin-film thermal characterization methods with an emphasis on identifying the properties extracted by the techniques. The characteristic timescale of heating and the geometry of the experimental structure govern the sensitivity of the data to the in-plane and out-of-plane conductivities, the volumetric heat capacity, and the interface resistances of the film. Measurement timescales and geometry also dictate the material volume probed most sensitively within the film. This article uses closed-form and numerical modeling to classify techniques according to the properties they measure. Examples of reliably extracted properties are provided for some experimental configurations. This article simplifies the process of choosing the best characterization technique for a given application in microdevice thermal design.

KEY WORDS: measurement techniques; metrology; thermal conductivity; thermometry; thin films.

1. INTRODUCTION

Knowledge of the thermal conduction properties of the solid films in integrated circuits and related devices is essential for effective design. As power densities continue to increase, the efficient conduction of heat away

[1] Invited paper presented at the Fourteenth Symposium on Thermophysical Properties, June 25–30, 2000, Boulder, Colorado, U.S.A.

[2] Department of Mechanical Engineering, Stanford University, Stanford, California, 94305-3030, U.S.A.

[3] To whom correspondence should be addressed.

0195-928X/01/0100-0243$19.50/0

from active regions is becoming a critical requirement. In some applications such as thermoelectric cooling and generation, radiation detection, and heat spreading in high-power devices, thermal conduction directly influences associated figures of merit. This makes these applications especially sensitive to variations in thermal properties of the component materials.

Thermal properties of materials in thin-film form in many cases differ strongly from those in bulk form [1]. In crystalline and polycrystalline dielectric and semiconducting films, heat conduction is dominated by transport of lattice vibrational waves, whose energy quanta are phonons. Phonon scattering on interfaces, imperfections accumulated during the material growth, and crystalline boundaries [1, 2] reduce the mean free path of heat carriers. This additional scattering can be directionally dependent, introducing anisotropy to the thermal conductivity. In noncrystalline solids, such as silicon oxides and nitrides, thermal conductivity and specific heat can also be process dependent, resulting from differences in structure, porosity, and sample stoichiometry [3, 4].

Heating and thermometry are the two essential actions in most thermal property measurements, and there is a variety of methods available for both actions. The relevance of a given technique for micromachined devices relies on the spatial and temporal resolution with which heating and thermometry are performed. As a result, it is useful to distinguish measurement techniques by (a) the method of heating, (b) the method of thermometry, and (c) the spatial and temporal resolution achieved by the measurement. These three distinguishing features of a given technique are linked, i.e., laser-based heating and thermometry techniques generally provide access to shorter timescales than electrical heating and thermometry using patterned microbridges.

While there is a variety of thin-film thermal characterization techniques available [5, 6], it is not always clear which technique is most appropriate for a given application. The precise thermal properties extracted using these methods vary depending on the timescale of the measurements and the geometry of the associated experimental structures. The data obtained using these techniques are influenced, often with undocumented relative strengths, by the in-plane and out-of-plane thermal conductivities of the film, the interface resistances, and the volumetric heat capacity. If the film is nonhomogeneous, the region governing the signal can vary strongly depending on the measurement technique. For these reasons, it is possible to extract thermal property data for a given film that are substantially different from those governing the temperature distribution in a given device containing that film. It is therefore important that measurements be tailored to yield a specifically targeted property needed in the design process. This review aims to help with this by investigating the impact of

measurement timescale and geometry on the sensitivities of the techniques to the in-plane and out-of-plane thermal conductivities, the volumetric heat capacity, and the interface resistances of the film.

We alert the readers to previous reviews of thermal property measurement techniques, which have had varying objectives. Cahill et al. [7] and Swartz and Pohl [8] discuss techniques suited particularly well for thermal property measurements of dielectric film geometries and their interfaces. Goodson and Flik [5] and Cahill [6] consider techniques relevant for electronic systems. Goodson and Ju [1] study thermal conduction in novel materials, with, an emphasis on the structural state of the films. Deposited diamond films were the subject of study by Graebner [9], Plamann and Fournier [10], and Touzelbaev and Goodson [11]. Almond and Patel [12] provide an extensive overview of photothermal techniques for thermal property measurements.

The goal of this article to is review existing thin-film thermal property measurement techniques, with an emphasis on the precise spatial and thermal property data obtained through the measurements. Compared to previous work, particular emphasis is placed on the extractable thermal property, which is directly affected by the measurement timescales and geometries. The considered timescales vary from the steady-state to deep sub-nanosecond regimes accessible using mode-locked lasers. The effects of the geometry of the heating source are also discussed. Additionally, this work provides examples of transient measurements in both frequency and time domains to illustrate dependence of the observed temperature response on both the thermal conductivity and the heat capacity of the measurement layer.

2. CLASSIFICATION OF MEASUREMENT TECHNIQUES

The methods of heating and thermometry vary greatly among available measurement techniques. The measured properties are strongly influenced by measurement timescales, in particular, the characteristic timescale of heating and the resolution of thermometry. This section briefly reviews existing heating and thermometry techniques and discusses the relevance of measurement timescales in determining which precise thermal properties are determined by a given technique.

2.1. Common Heating and Thermometry Methods

The heat flux in the most common techniques is induced either by Joule heating [13–25] or by absorption of electromagnetic radiation [26–37]. The advantage of Joule heating techniques is precise knowledge

of the deposited heating power. The disadvantages of Joule heating methods include the need for fabrication of special measurement structures on the sample surface and their electrical isolation from the sample, if it is electrically conducting. In the case of heating by absorption of electromagnetic radiation, the sample often needs no additional or a very minimal amount of preparation, typically the deposition of a metal film on the surface of the sample. Optical techniques offer the potential for development of high-throughput noncontact measurement systems suited particularly well for thermal characterization of novel materials whose chemical and structural stability during the standard fabrication procedures is often not available. However, the amount of the absorbed radiation power is very difficult to quantify. In this case only the relative temperature response at the surface of the sample at several heating frequencies can be used to extract thermal properties of underlying layers, as discussed in subsequent sections.

Steady-state techniques (e.g., Refs. 7, 13, and 14), generally require knowledge of two or more temperatures at precisely defined positions within the measurement structure. In contrast, transient techniques, in principle, do not require temperature measurements at two different locations, if the thermal diffusion length at measurement timescales does not exceed dimensions of the experimental structure. One of the most common and accurate techniques is electrical resistance thermometry [13–25], which can be precisely calibrated. The other common technique, thermoreflectance thermometry (e.g., Refs. 26–33), uses the temperature dependence of optical reflectivity to detect changes in the temperature of the sample surface. The advantage of thermoreflectance thermometry is that it requires neither contact with the sample nor extensive sample preparation. At most the measurement necessitates deposition of a thin reflective coating. The disadvantage is that the samples have to be sufficiently reflective to collect a satisfactory amount of radiation at the detector. Due to the small value of the thermoreflectance coefficient, which is of the order of 10^{-4} to $10^{-6}\,K^{-1}$ for metals at room temperature, such measurements require averaging or lock-in detection, or a combination of both [29], to improve the signal-to-noise ratio.

2.2. Measurement Timescale

Many techniques measure temperatures at the heating location, which in this paper is assigned a coordinate $r = 0$ for convenience, where the temperature rise is highest and easiest to measure. Examples of this type of techniques are the 3-ω technique [17–25], performed in the frequency domain, and purely optical techniques [26–33], performed in the time

domain, for normal property measurements. Figure 1 shows the temperature response as a function of frequency for a representative multilayer. In this geometry, the heat is absorbed on the surface of a 100-nm-thick layer, which has an acoustic mismatch thermal resistance with the next 1-μm-thick layer of high thermal conductivity. Femtosecond laser heating and thermometry [29–33] detect this regime of heat diffusion particularly well and were successfully applied for measurements of acoustic mismatch resistance between the metal absorption layer and the high-thermal conductivity sample, as well as the sample thermal conductivity. Nanosecond laser thermometry can also be applied at these measurement frequencies, as illustrated by the work of Verhoeven et al., [27, 28], which measured the thermal properties of highly- oriented CVD-diamond layers with the thermal conductivity normal to layers approaching 600 $W \cdot m^{-1} \cdot K^{-1}$. There can be considerable thermal diffusion during the nanosecond-range pulses, and, therefore, the analysis of the thermal signal will have to involve the temporal pulse shape of the heating laser.

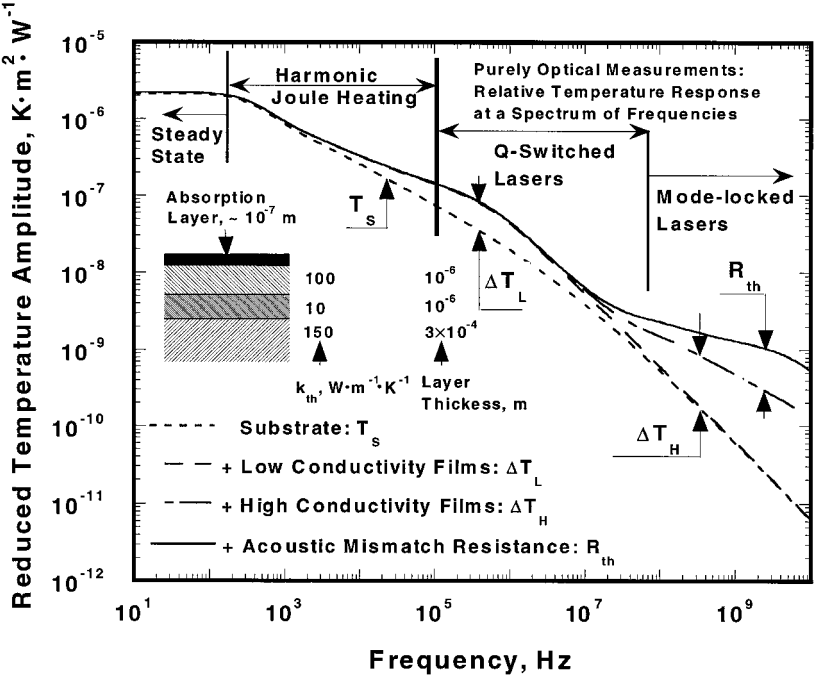

Fig. 1. Frequency range of most common types of heating and thermometry. Layers whose internal or boundary thermal properties govern the surface temperature response change with the measurement frequency.

At longer timescales, heat further diffuses into the substrate through the low-thermal conductivity film. Due to the high repetition rate, the mode-locked lasers are often not suited for measurements in the considered regime. Both nanosecond laser thermometry and harmonic Joule heating techniques possess the relevant frequency range and have been applied extensively for these types of measurements. The electrical methods are most accurate but offer a limited measurement frequency range. These low frequencies make transient Joule heating techniques suitable for the measurements of substrate properties and films of low thermal conductivity.

In contrast to techniques presented in Fig. 1, the technique of Hatta [38] and the mirage technique of Boccara et al. [39], along with other related methods [40–47], use phase delay of the temperature response under periodic heat flux at a location removed from the heating source, $r > 0$. The measurements can also be done in the time domain, as in the laser flash technique of Shibata et al. [48] and the thermal grating techniques of Kaeding et al. [35, 36]. Both are based on measuring the characteristic rise time at a location removed from the point of maximum heat flux. Due to the nature of phase delay techniques, the heat capacity of measured samples cannot be decoupled from their resistance, so typically the measured parameter is the ratio of one conductivity component and the volumetric heat capacity, or a directional thermal diffusivity. A more complete discussion of these techniques is given in the next section.

3. ANALYSIS

This section introduces analytical solutions to the heat conduction equation, which are used for thermal property extraction. The solutions are obtained using Fourier transforms in space and time, an approach that is especially helpful for techniques using temporally- or spatially- harmonic heating sources. Under a temporally harmonic, or periodic, heating source $P(\vec{r}, \omega)\cos(\omega t + \varphi_0)$, where $\omega = 2\pi f$ is the angular frequency and φ_0 is the initial phase, the general expression for temperature response is

$$\begin{aligned} T(\vec{r}, \omega, t, \varphi_0) &= T_R(\vec{r}, \omega)\cos(\omega t + \varphi_0) + T_C(\vec{r}, \omega)\sin(\omega t + \varphi_0) \\ &= T_A(\vec{r}, \omega)\cos(\omega t + \varphi_0 - \Delta\varphi(\vec{r}, \omega)) \end{aligned} \tag{1a}$$

Variables T_R and T_C are often referred to as resistive and capacitive components of the temperature, respectively, and $T_A = \sqrt{T_R^2 + T_C^2}$ and $\Delta\varphi = \tan^{-1}(T_C/T_R)$ are the amplitude and phase delay of the temperature.

In practice, heating is never negative due to always-present steady-state components of heat generation, but the linearity of the heat conduction

equation with temperature-independent thermal properties allows decoupling of the response to the periodic component of the heating source. Frequency-domain experimental techniques measure the frequency- dependence of the magnitude of T_A and phase delay $\Delta\varphi$, usually using lock-in amplifiers. One approach to interpreting the data is to solve a set of separate differential equations for T_R and T_C. A simpler approach uses complex imbedding [49] to express the heating source as $P\exp[i(\omega t+\varphi_0)]$, where $i=\sqrt{-1}$. The solutions, obtained under such a source, incorporate both T_R and T_C components of the temperature rise into a single complex variable $\theta(\vec{r},\omega)=T_R(\vec{r},\omega)-iT_C(\vec{r},\omega)=T_A(\vec{r},\omega)\exp[-i\Delta\varphi(\vec{r},\omega)]$. This approach has grown more practical with the development of mathematics and programming software capable of handling complex numbers. Once the solution is obtained, the temperature can be reconstructed as

$$T(\vec{r},\omega,t,\varphi_0)=\mathrm{Re}\{\theta(\vec{r},\omega)\exp[i(\omega t+\varphi_0)]\} \tag{1b}$$

which is entirely equivalent to Eq. (1a). For temporally periodic problems forced by a cosine source function, this work presents complex solutions for $\theta(\vec{r},\omega)$, which are to be translated into real temperatures using Eq. (1b).

The first subsection provides solutions for semiinfinite media, which are useful for interpreting both in-plane and out-of-plane conductivity measurement data. The second subsection provides more detailed analysis of conduction in multilayer structures.

3.1. Solutions for Semi-Infinite Media

Plane, line, or point sources can approximate the geometry of induced heat flux in many experimental techniques. The solutions are readily available [49]:

$$\theta_{\text{plane}}(r,\omega)=\frac{P}{A}\frac{\exp(-pr)}{pk} \tag{2a}$$

$$\theta_{\text{line}}=\frac{P}{\pi L}\frac{K_0(pr)}{k} \tag{2b}$$

$$\theta_{\text{point}}(r,\omega)=\frac{P}{2\pi}\frac{\exp(-pr)}{kr} \tag{2c}$$

where $p=(1+i)/L_{\text{th}}$, $L_{\text{th}}=\sqrt{2\alpha/\omega}$ is the thermal diffusion length, k and α are the thermal conductivity and diffusivity, L is the length of the line for the line source, K_n is the modified Bessel function of order n, and A is the area of the plane source.

Equations (2) contain parameter p, which is directly related to the thermal diffusivity of samples, $\alpha = k/C_V$, where C_V is the heat capacity per unit volume. As mentioned in Section 2, there is a class of measurement techniques [38–47] which is based on acquiring a value of p and, therefore, the diffusivity of the sample. For convenience, one can introduce non-dimensional parameters G and H, defined as

$$G = \frac{r}{\theta}\frac{\partial \theta}{\partial r} = \frac{\partial \ln(\theta)}{\partial \ln(r)} = \frac{\partial \ln(T_A)}{\partial \ln(r)} - i\frac{\partial \Delta\varphi}{\partial \ln(r)} \tag{3a}$$

$$H = \frac{\partial \ln(\theta)}{\partial \ln(\omega)} = \frac{\partial \ln(T_A)}{\partial \ln(\omega)} - i\frac{\partial \Delta\varphi}{\partial \ln(\omega)} \tag{3b}$$

Values of both the real components, which are governed by the temperature amplitude, and the imaginary components, which are governed by the phase delay, of G and H can be experimentally determined by varying the position or frequency of the measurement. Table I shows analytical expressions for these parameters, depending only on the non-dimensional variable $p \times r$, which can be fitted to the experimental data and yield the thermal diffusivity of the sample. The absolute values of heat flux and temperature are not needed, and the only requirements are the sufficient bandwidth and the linear response of the thermometry technique over the temperature and frequency range encountered in the experiment. It is clear that at the position $r = 0$, G and H have no dependence on p, which makes

Table I. Mathematical Expressions for Analysis of Experimental Data Directly Governed by the Sample Thermal Diffusivity α (Section 3.1)[a]

	Source geometry for analysis	
	$G(r,\omega) = \frac{r}{\theta}\frac{\partial \theta}{\partial r}$	$H(r,\omega) = \frac{\omega}{\theta}\frac{\partial \theta}{\partial \omega}$
Plane	$-pr$	$-0.5(pr+1)$
Line	$-pr\frac{K_1(pr)}{K_0(pr)}$	$-0.5pr\frac{K_1(pr)}{K_0(pr)}$
Point	$-pr-1$	$-0.5-pr$

[a] Thermal diffusivity is related to the parameter $p = (1+i)/L_{\text{th}}$, where $L_{\text{th}} = \sqrt{2\alpha/\omega}$. Experimental values of functions G and H can be determined from temperatures taken at varying positions or frequencies. The assumed geometry is semiinfinite.

these techniques use measurements of temperature at the location $r \neq 0$ some distance, comparable to L_{th}, away from the heater.

The other class of techniques, not necessarily implemented in semi-infinite geometry, [17–25], which requires absolute magnitudes of temperature and heat flux, uses measurements at $r \approx 0$. For small values of z in semiinfinite geometry, one can write [50] $K_0(z) - \gamma + \ln(2) - \ln(z)$, where γ is the Euler constant, and $\exp(-z) \sim 1 - z$ to obtain the functional dependence of the surface temperature on the measurement angular frequency as

$$\theta_{plane}(\omega) = \frac{P}{A}\frac{1-i}{\sqrt{2}} k^{-1}\alpha^{1/2}[\omega^{-1/2}] \tag{4a}$$

$$\theta_{line}(\omega) = \frac{P}{L}\frac{1}{2\pi} k^{-1}[-\ln(\omega)] + C \tag{4b}$$

$$\theta_{point}(\omega) = P\frac{1}{2\pi}\frac{(1+i)}{\sqrt{2}} k^{-1}\alpha^{-1/2}[\omega^{1/2}] + C \tag{4c}$$

where C is the constant independent of frequency. These results are summarized in Table II. In the case of point and plane sources, both in-phase and out-of-phase components can be used to evaluate a corresponding combination of thermal properties.

Table II. Mathematical Expressionsx for Analysis of the Experimental Temperature Response Obtained at the Location of the Heat Source, $r = 0$ (Section 3.1)[a]

	Idealized source geometry		
	Plane	Line	Point
Extracted property	$k\alpha^{-0.5}$	k	$k\alpha^{0.5}$
Functional dependence, $F(\omega)$	$\omega^{-0.5}$	$\ln(\omega)$	$\omega^{0.5}$
In-phase slope of Temperature as a function of $F(\omega)$	$\frac{P}{\sqrt{2}\,A} k^{-1}\alpha^{0.5}$	$-\frac{P}{(\sqrt{2})^2\,\pi L} k^{-1}$	$-\frac{P}{(\sqrt{2})^3\,\pi} k^{-1}\alpha^{-0.5}$
Out-of-phase slope of Temperature as a function of $F(\omega)$	$-\frac{P}{\sqrt{2}\,A} k^{-1}\alpha^{0.5}$	0	$-\frac{P}{(\sqrt{2})^3\,\pi} k^{-1}\alpha^{-0.5}$

[a] The assumed geometry is semiinfinite.

For measurements performed in the time domain, the surface temperature can be determined from the frequency components of the heating power and corresponding solutions to the heat equation. For the case of one-dimensional heat flow in the plane source geometry, the temperature at the surface, provided that the heating power $P(t)$ is an even function of time $P(t) = P(-t)$ to satisfy $\varphi_0 = 0$, is

$$T(t) = \frac{1}{2\pi} k^{-1} \alpha^{1/2} \int_{-\infty}^{\infty} \left[\frac{P(\omega)}{A} \frac{\cos(\omega t)}{\sqrt{2\omega}} \right] d\omega \tag{5a}$$

where

$$P(\omega) = \int_{-\infty}^{\infty} P(t) \cos(\omega t)\, dt \tag{5b}$$

There is also a class of techniques [26–34] which measure temperatures at $r \approx 0$, but do not require absolute values of temperature and heat flux. In purely optical thermoreflectance techniques, a high-thermal conductivity metal layer is typically deposited on top of the sample. The metal layer serves two purposes: one is to absorb radiation from the pump beam, and the second is to provide the needed thermal property contrast with the measured layer. Solutions in the multilayer geometry are required for the analysis of such techniques.

3.2. Heat Conduction in Multilayer Systems

This section provides transient solutions to the three-dimensional heat conduction equation in a multilayer with a number of layers $N > 1$. This is important because many thin-film property measurements are performed in a geometry with multiple layers surrounding the layer of interest. Coordinate z_n within each layer varies between 0 and L_n, where L_n is the thickness of the nth layer, while both x and y coordinates are common to all layers and extend to infinity. The volumetric heat generation rate in each layer, $\dot{q}_n \exp\lfloor i(\omega t + q_x x + q_y y)\rfloor$, is assumed to be independent of z_n. The general solution is

$$\theta_n(z, q_x, q_y, \omega) = \frac{\dot{q}_n}{p_n^2 k_{z,n}} + C_{A,n} \sinh(p_n z_n) + C_{B,n} \cosh(p_n z_n); \qquad 1 \leqslant n \leqslant N \tag{6}$$

where $p_n = \sqrt{i\omega/\alpha_{z,n} + r_{x,n}q_x^2 + r_{y,n}q_y^2}$, $k_{z,n}$ and $a_{z,n}$ are the thermal conductivity and the thermal diffusivity, respectively, in the z-direction in the nth layer, i is the imaginary unit, $r_{x,n} = k_{x,n}/k_{z,n}$, $r_{y,n} = k_{y,n}/k_{z,n}$, and q_x and q_y are wavenumbers along the x and y coordinates, respectively.

Assuming an insulated boundary at $z_1 = 0$, free coefficients for $n = 1$ are

$$\vec{\mathbf{C}}_1 = \begin{bmatrix} C_{A,1} \\ C_{B,1} \end{bmatrix} = \begin{bmatrix} 0 \\ -\dfrac{a_1 \tanh^s(p_N L_N) + a_2}{b_{1,2}\tanh^s(p_N L_N) + b_{2,2}} \end{bmatrix} \tag{7}$$

where $s = 1$ for the case of the zero temperature imposed at $z_N = L_N$ and $s = -1$ for the insulated boundary condition at $z_N = L_N$, a_m are elements of the vector $\vec{\mathbf{A}} = \sum_{n=2}^{N} \mathbf{P}_{N-n}\vec{\mathbf{S}}_{n-1}$, and $b_{m,n}$ are elements of the of the matrix $\mathbf{B} = \mathbf{P}_{N-1}$. The vector $\vec{\mathbf{S}}_n$ is given by

$$\vec{\mathbf{S}}_n = \begin{bmatrix} 0 \\ \dfrac{\dot{q}_n}{p_n^2 k_{z,n}} - \dfrac{\dot{q}_{n+1}}{p_{n+1}^2 k_{z,n+1}} \end{bmatrix}; \qquad 1 \leqslant n < N \tag{8}$$

Matrices $\mathbf{P}_n$ for $n > 0$ can be defined by recursive relations

$$\begin{aligned} \mathbf{P}_0 &= \mathbf{E} \\ \mathbf{P}_1 &= \mathbf{M}_{N-1} \\ \mathbf{P}_n &= \mathbf{P}_{n-1}\mathbf{M}_{N-n}; \qquad 1 < n < N \end{aligned} \tag{9}$$

where $\mathbf{E}$ is an identity matrix. Transfer matrices $\mathbf{M}_n$ are obtained as

$$\mathbf{M}_n = \begin{bmatrix} \dfrac{k_{z,n}p_n}{k_{z,n+1}p_{n+1}}\cosh(p_n L_n) & \dfrac{k_{z,n}p_n}{k_{z,n}p_{n+1}}\sinh(p_n L_n) \\ \sinh(p_n L_n) + R_n k_{z,n} p_n \cosh(p_n L_n) & \cosh(p_n L_n) + R_n k_{z,n} p_n \sinh(p_n L_n) \end{bmatrix}; \qquad 1 \leqslant n < N$$

where R_n is the thermal boundary resistance between the layers n and $n+1$. Free coefficients in the nth layer can be calculated using recursive relations $\vec{\mathbf{C}}_{n+1} = \mathbf{M}_n\vec{\mathbf{C}}_n + \vec{\mathbf{S}}_n$, $1 \leqslant n < N$.

Using inverse Fourier transforms, the temperature in the time–space domain is obtained as

$$T_n(t, x, y, z) = \mathrm{Re}\{\mathscr{F}^{-1}_{q_x, q_y, \omega}[\theta_n(\omega, z, q_x, q_y)]\} \tag{11a}$$

where $\mathscr{F}^{-1}_{q_x, q_y, \omega}$ indicates the inverse Fourier transform. Heat generation rates in the frequency–wavenumber space are obtained by direct Fourier transform,

$$\dot{q}_n(\omega, q_x, q_y) = \mathscr{F} \tag{11b}$$

4. STEADY-STATE TECHNIQUES

Achieving an adequate spatial resolution is particularly important for the steady-state techniques, which generally require knowledge of two temperatures at precisely defined positions within the measurement structure. The geometry of the measurement in well-designed steady-state techniques meets three requirements. First, thermal resistance between the measurement positions is governed by or has a substantial dependence on thermal conduction in the layer of interest. Second, this resistance has very little or no dependence on thermal conduction to the environment once heat flows out of the measurement structure. Finally, thermal resistance between the measurement locations has to be, at least, comparable to the total thermal resistance to the environment or heat sink in order to reduce measurement errors.

4.1. Conductivity Normal to Layers

An example of the spatially resolved approach to measure thermal conduction properties normal to layers is a technique used by Swartz and Pohl [13] to measure thermal boundary resistance between the metal and the substrate. Both heater and thermometer lines were placed parallel to each other on the top of the substrate. The small separation between the lines makes the difference in their temperatures be governed not only by the thermal properties of the substrate, but also by the thermal resistance between the metal film and the substrate, which subsequently can be extracted if substrate properties are known. Placing the thermometer line closer to the heater line allows measuring lower values of thermal resistance and reduces the sensitivity of the measurement to the substrate thermal properties. This technique was later modified by Cahill [7] to measure thermal resistances of oxide films sandwiched between metal and

substrate, $R_{th} = d/k$, where d is the film thickness and k is its thermal conductivity. Goodson [51] provided a correction for films whose thickness is comparable to the heater width, w, where lateral spreading can be substantial. Thermal resistance is $R_{th} = d/(k\Psi)$, where

$$\Psi = \left[1 - 0.54276 \frac{1 - 0.932 \exp(-1.538(w/d))}{w/d} \right]^{-1} \tag{12}$$

which is within 0.5% for $w/d > 0.6$

Schafft et al. [15] and Brotzen et al. [16] also used metal bridges to measure k_n for amorphous silicon dioxide films. Both techniques employ only a single bridge, which makes it difficult to decouple thermal resistance due to the measured layer from the overall thermal resistances to the environment or heat sink. Accordingly, these techniques are suited only for the case when film thermal resistance dominates the overall resistance to the heat sink/environment or when components of the thermal resistance other than the film resistance are known or predicted using the necessary assumptions.

4.2. Conductivity Along Layers

Steady-state techniques for thermal conductivity measurement are well developed and have been reviewed by Goodson and Flik [5]. Most of these techniques suspend the layers of interest, which forces one-dimensional heat flow in the film. Another technique [14] uses a high-thermal resistance layer with known properties between the substrate and the measured film, which also forces one-dimensional heat flow along the film. Any measurement errors in the thickness of the film directly affect the extracted property, since these techniques measure film conductance, $k_a \times d$.

It is also possible to force heat flow spreading in the film by making the strip heater width comparable to the film thickness. If the film is isotropic and its out-of-plane thermal conductivity is known, the reduction of film thermal resistance due to spreading can be obtained using the approximation given by Eq. (12); otherwise, the film is anisotropic. No mention of such steady-state techniques has been found in the literature.

5. FREQUENCY DOMAIN TECHNIQUES

Harmonic Joule-heating techniques, particularly the 3-ω technique, have become very popular in the past few years. Most common applications, which are well documented in the literature, involve measurements of bulk thermal conductivity in the line-source geometry and measurement of

the thermal resistance of thin dielectric films with a low thermal conductivity. In this section we concentrate on some less common experimental configurations, which can also find applications in thin-film thermal property metrology.

5.1. Plane- and Point-Source Semiinfinite Geometries

The plane-source solution is well suited for the geometry of the suspended film. Figure 2 shows the data and the fit using Eq. (4a). The data are taken from a 3-μm-thick suspended film, which in this particular case is a SiGe superlattice layer. Both in-phase and out-of-phase components, as discussed in Section 3, can be used to extract the thermal product of the measured material. This feature can be useful in the uncertainty analysis. For this layer, the film heat capacity was available, which resulted in an extracted thermal conductivity of 13.5 $W \cdot m^{-1} \cdot K^{-1}$ at room temperature. If the heat capacity is unknown, one can complement this measurement with the phase delay technique to obtain values of the thermal diffusivity, as discussed in Section 3.

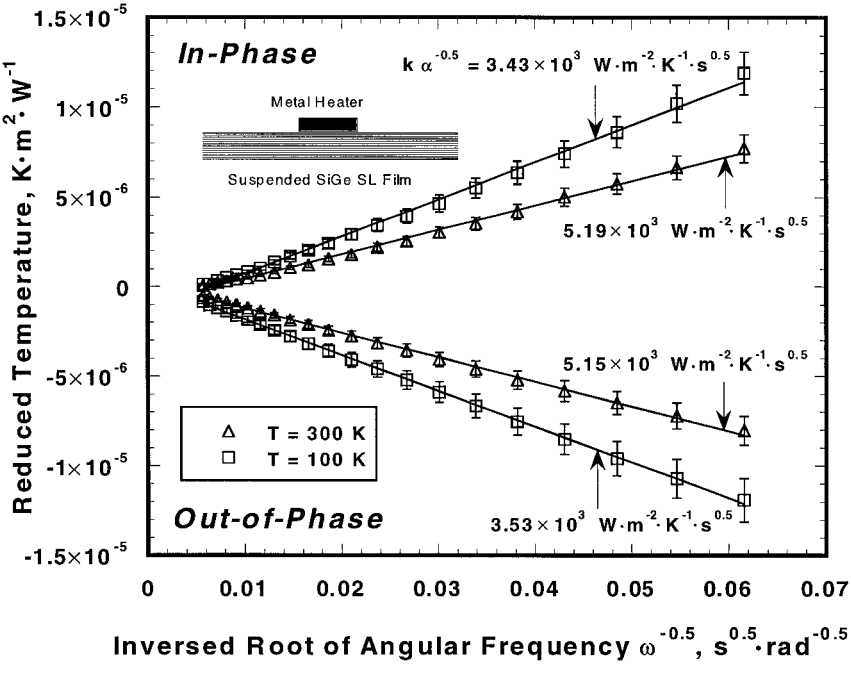

Fig. 2. Example of 3-ω measurements with a plane heating source. The extraction procedure used an expression given in Table II.

Recently developed techniques can induce local heating in the geometry of a point source and thus achieve a high spatial resolution in mapping sample thermal properties [52–55]. One promising example is the study by Fiege et al. [56], which applied local harmonic-heating generated in a resistive element with a contact area dimension of about 30 nm along the surface of diamond layer. The effects of contact topography, which governs the thermal contact resistance between the heater and the layer, can easily be decoupled, since it results in frequency-independent contributions to the thermal signal. By directly comparing their data with the data taken on material with known thermal properties, Fiege et al. [56] spatially mapped the thermal conductivity of thick CVD-diamond film. Their work demonstrated an extension of the 3-ω technique to the point source geometry; however, the extraction of data using the line-source solution may have contributed to the overall errors.

5.2. Multilayer Geometry

Harmonic Joule-heating techniques are used extensively to study thermal conductivities of thin dielectric layers [19–25]. At measurement frequencies below the heat diffusion frequency of the film, the slope $d\theta/d\ln(\omega)$ still depends on the substrate thermal conductivity, while there is an additional frequency independent component due to thermal resistance of the thin film. The geometry of the measurement can be modified to accommodate measurements of the lateral thermal conductivity of the layer [22, 24], if the width of the line is comparable to the thickness of the measured layer. In that case, the resistance of the layer also becomes a function of the lateral conductivity. Typically it is more convenient to measure normal properties by using a wider line to reduce uncertainties. Figure 3 demonstrates measurement of both normal and lateral components of polymer thermal conductivity using this approach [24]. The exact experimental geometry was captured in the numerical simulations, which used finite differences with complex imbedding.

6. TIME DOMAIN TECHNIQUES

Thermoreflectance measurements, which use pulsed lasers, are examples of time-domain techniques. In the most common experimental configuration, a thin layer with a high thermal resistance is sandwiched between the substrate and the thick deposited metal. The property extracted in this technique is the thermal resistance of the layer [6, 26, 34]. Stoner and Maris [30] performed a related measurement, which used mode-locked

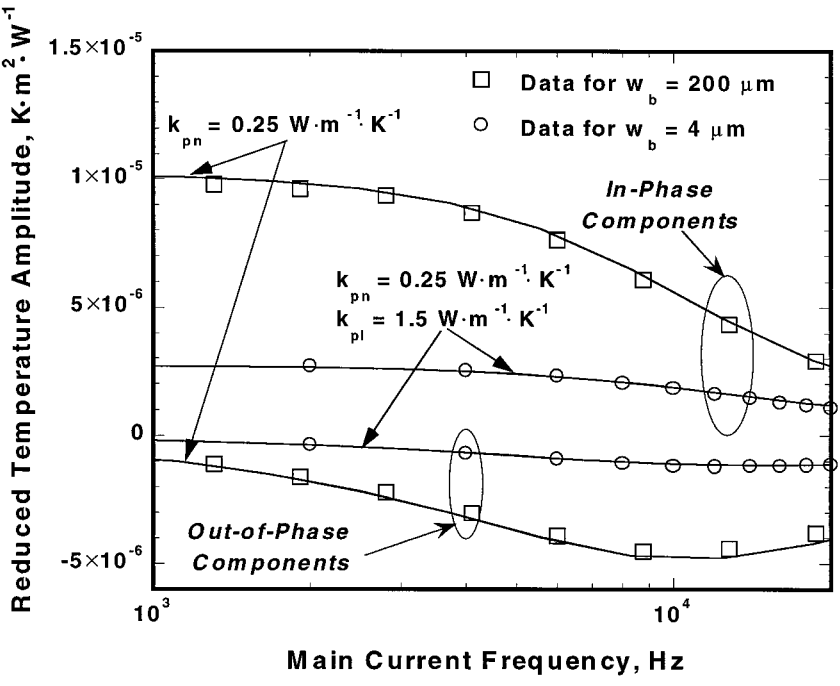

Fig. 3. Example of 3-ω measurements sensitive to lateral heat spreading in the measured layer. The resistance of the polymer film in the case of localized heating whose extent is comparable to the film thickness, is a function of both normal and lateral components of the conductivity tensor.

lasers, where the property of interest was the Kapitza resistance between the metal and the diamond. Due to the high thermal conductivity, thermal conduction in diamond contributes negligibly to the surface temperature rise and may be omitted in the data analysis. In this section we consider other experimental configurations, which have received less attention but can be useful in many applications.

6.1. Semiinfinite Geometry

One-dimensional conduction in a semiinfinite medium can be modeled by considering an equivalent thermal circuit, shown on the left in Fig. 4. The time-dependent response of this circuit, which has frequency-dependent resistance and capacitance, can be exactly described by the solution to the plane source heat conduction equation, given in Section 3. Figure 4 also shows that the characteristic RC timescale of this circuit is independent of

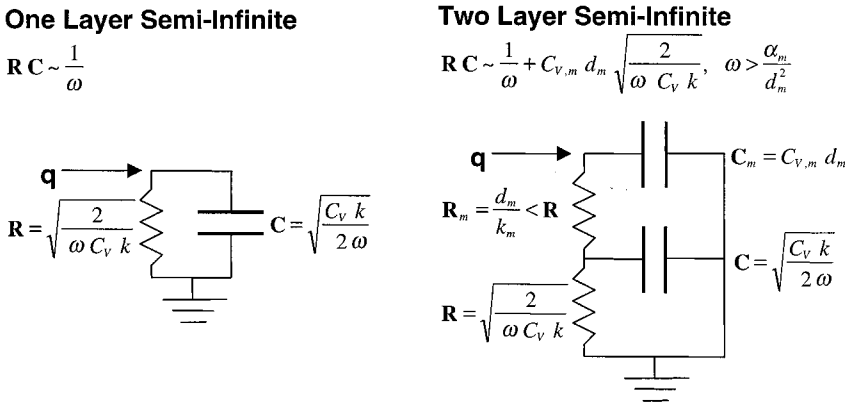

Fig. 4. Equivalent thermal circuit representation of heat conduction in a thin film–substrate system. The thermal circuit on the left models the temperature response of a semi-infinite medium to a plane source with angular frequency ω. The *RC* timescale of this circuit is independent of the substrate thermal properties. The addition of a layer with a much higher thermal conductivity and known heat capacitance allows measurements of the substrate thermal properties. Figure 5 shows an example of such measurement.

the material property. By introducing a high-conductivity metal layer, an additional thermal capacitor of known value is added to the thermal circuit, as shown on the right in Fig. 4. Thermal excitation frequencies higher than $\omega - \alpha_m/d_m^2$ will result in a temperature response governed predominantly by the metal overlayer. At lower measurement frequencies, the *RC* timescale of such a circuit is most sensitive to the thermal product of the substrate and the volumetric thermal heat capacity and thickness of the metal, as shown in Fig. 4. The uncertainty in the thickness of the metal layer can contribute substantially to the overall uncertainty of the measurement since the measured property combination $(C_{V,m}\, d_m)^2/(k_S \rho_S)$ contains the square of the metal thickness.

Figure 5 shows the thermoreflectance signal obtained from the thick polymer layer and results of fitted solutions to the heat conduction equation in the appropriate geometry. The values of the thermal heat capacity of the substrate and thickness of the metal were varied over a wide range and resulted in values of the fitted thermal conductivity of the substrate which satisfied the relation $d^2 k_S^{-1} \rho_S^{-1} = \text{const}$ in accordance with the simplified thermal circuit analysis.

6.2. Measurements of Thin-Film Properties

Figure 6 shows the experimental data and the fit for the three-layer case when the thickness of the measured layer is comparable to the thickness

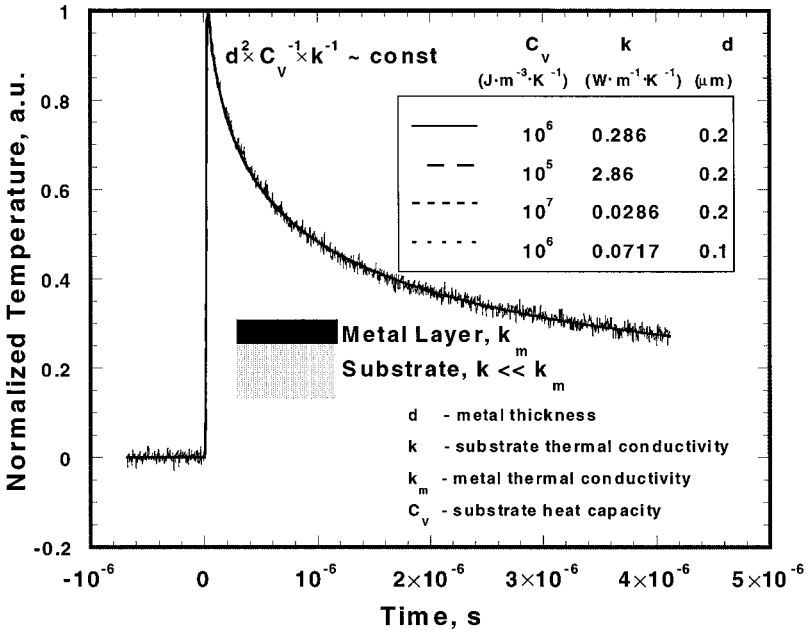

Fig. 5. Example of thermoreflectance measurements on a metal film/substrate system. Extraction of a substrate thermal conductivity requires precise knowledge of the substrate and metal heat capacities, as well as of the metak thickness. See Fig. 4 for the equivalent thermal circuit representation.

of the top metal layer. This represents an intermediate case between the measurements of the thermal resistance and those of the thermal properties in a semiinfinite medium, which was considered in the preceding paragraph. The decaying temperature can be subdivided into two regimes. At high frequencies/short timescales, thermal conduction can be viewed to be semi-infinite in the layer and, therefore, has sensitivity on both thermal conductivity and heat capacity, as discussed in the previous subsection. At longer timescales, i.e., $t = d^2/\alpha$, the sensitivity will be mostly on the thermal conductivity of the layer. By choosing the length of the measurement, one can correspondingly increase or decrease the sensitivity of the fit on the heat capacity of the film. For the case presented in Fig. 6, the total length of the measurement is about three times longer than the diffusion time through the film, which greatly diminishes the sensitivity of the fit on the heat capacity of the film. Decreasing the heat capacity of the film from the best-fit value of 1.5 $MJ \cdot m^{-3} \cdot K^{-1}$ by 33% resulted in a corresponding change in the thermal conductivity by only less than 3%.

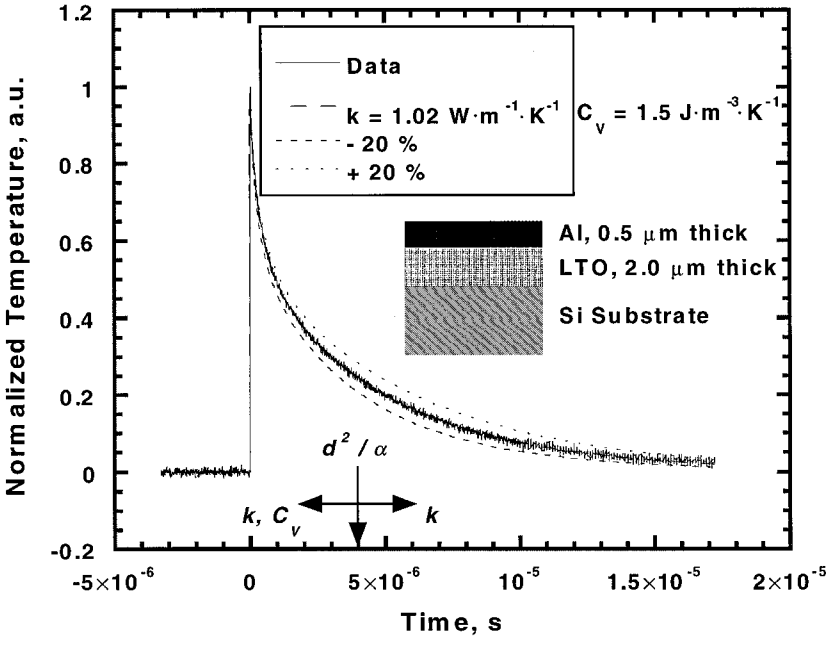

Fig. 6. Example of thermoreflectance measurements on a metal/measured layer/substrate system. In the initial stages of the temperature decay, the heat capacity of the measured film is important, as in the case shown in Fig. 5.

7. CONCLUSIONS

This work provides an overview of techniques for measuring material thermal properties based on the geometry and timescale of the experiment. The timescale of these measurement techniques varies widely from steady-state to short-timescale heat conduction regimes, accessible through laser heating and thermometry. Accordingly, each of these techniques has different application ranges (Fig. 1).

This work has discussed some common experiments in which the layer thermal conductivity and heat capacity influence, with varying strengths, the measured temperature response. Using both harmonic Joule-heating and optical techniques, we have also provided several examples which involve experimental configurations not yet well documented in the literature.

REFERENCES

1. K. E. Goodson and Y. S. Ju, *Annu. Rev. Mater. Sci.* **29**:261 (1999).
2. J. M. Ziman, *Electrons and Phonons* (Oxford University Press, Oxford, 1960), pp. 450–474.

3. K. E. Goodson, M. I. Flik, S. T. Su, and D. A. Antoniadis, *ASME J. Heat Transfer* **116**:317 (1994).
4. Y. S. Ju and K. E. Goodson, *J. Appl. Phys.* **85**:7130 (1999).
5. K. E. Goodson and M. I. Flik, *Appl. Mech. Rev.* **47**:101 (1994).
6. D. G. Cahill, *Microsc. Therm. Eng.* **1**:85 (1997).
7. D. G. Cahill, H. E. Fischer, T. Klitsber, E. T. Swartz, and R. O. Pohl, *J. Vac. Sci. Technol. A* **7**:1259 (1989).
8. E. T. Swartz and R. O. Pohl, *Rev. Modern Phys.* **61**:605 (1989).
9. J. E. Graebner, *Diamond Films Technol.* **3**:77 (1993).
10. K. Plamann and D. Fournier, *Diamond Rel. Mater.* **4**:809 (1995).
11. M. N. Touzelbaev and K. E. Goodson, *Diamond Rel. Mater.* **7**:1 (1998).
12. D. P. Almond and P. M. Patel, *Photothermal Science and Techniques* (Chapman Hall, London, 1996), pp. 199–217.
13. E. T. Swartz and R. O. Pohl, *Appl. Phys. Lett.* **51**:2200 (1987).
14. M. Asheghi, M. N. Touzelbaev, K. E. Goodson, Y. K. Leung, and S. S. Wong, *ASME J. Heat Transfer* **120**:30 (1998).
15. H. A. Schafft, J. S. Suehle, and P. G. A. Mirel, *Proc. IEEE Int. Conf. Microelectron. Test Struct.* **2**:121 (1989).
16. F. R. Brotzen, P. J. Loos and D. P. Brady, *Thin Solid Films* **207**:197 (1992).
17. D. G. Cahill, *Rev. Sci Instrum.* **61**:802 (1990).
18. D. G. Cahill and R. O. Pohl, *Phys. Rev. B* **35**:4067 (1987).
19. D. G. Cahill and T. H. Allen, *Appl. Phys. Lett.* **65**:309 (1994).
20. D. G. Cahill, M. Katiar, and J. R. Abelson, *Phys. Rev. B* **50**:6077 (1994).
21. S.-M. Lee and D. G. Cahill, *J. Appl. Phys.* **81**:2590 (1997).
22. K. Kurabayashi, M. Asheghi, M. Touzelbaev, and K. E. Goodson, *J. Microelectromech. Syst.* **8**:180 (1999).
23. Y. S. Ju and K. E. Goodson, *J. Appl. Phys.* **85**:7130 (1999).
24. K. Kurabayashi, M. Touzelbaev, M. Asheghi, Y. S. Ju, and K. E. Goodson, submitted for publication.
25. J. H. Kim, A. Feldman, and D. Novotny, *J. Appl. Phys.* **86**:3959 (1999).
26. O. W. Kaeding, H. Skurk, and K. E. Goodson, *Appl. Phys. Lett.* **65**:1629 (1994).
27. H. Verhoeven, E. Boettger, A. Flöter, H. Reiß, and R Zachai, *Diamond Relat. Mater.* **6**:298 (1997).
28. H. Verhoeven, A. Flöter, H. Reiß, R Zachai, D. Wittorf, and W. Jäger, *Appl. Phys. Lett.* **71**:1389 (1997).
29. W. S. Capinski and H. J. Maris, *Rev. Sci. Instrum.* **67**:2720 (1996).
30. R. J. Stoner and H. J. Maris, *Phys. Rev. B* **48**:16373 (1993).
31. W. S. Capinski, H. J. Maris, E. Bauser, I. Silier, M. Asen-Palmer, T. Ruf, M. Gardona, and E. Gmelin, *Appl. Phys. Lett.* **71**:2109 (1997).
32. W. S. Capinski, H. J. Maris, E. Bauser, T. Ruf, M. Gardona, K. Ploog, and D. S. Katzer, *Phys. Rev. B* **59**:8105 (1999).
33. C. J. Morath, H. J. Maris, J. J. Cuomo, D. L. Pappas, A. Grill, V. P. Patel, J. P. Doyle, and K. L. Saenger, *J. Appl. Phys.* **76**:2636 (1994).
34. G. Chen and P. Hui, *Thin Solid Films* **339**:58 (1998).
35. O. W. Kaeding, H. Skurk, A. A. Maznev, and E. Matthias, *Appl. Phys. A* **61**:253 (1995).
36. O. W. Kaeding, E. Matthias, R. Zachai, H.-J. Füßer, and P. Münzinger, *Diamond. Relat. Mater.* **2**:1185 (1993).
37. J. E. Graebner, *Rev. Sci. Instrum.* **66**:3903 (1995).
38. I. Hatta, *Rev. Sci Instrum.* **56**:1643 (1985).
39. A. C. Boccara, D. Fournier, and J. Badoz, *Appl. Phys. Lett.* **36**:130 (1980).

40. T. Yao, *Appl. Phys. Lett*. **51**:1798 (1987).
41. E. P. Visser, E. H. Versteegen, and W. J. P. van Enckevort, *J. Appl. Phys*. **71**:3238 (1992).
42. G. Chen, C. L. Tien, X. Wu, and J. S. Smith, *ASME J. Heat Transfer* **116**:325 (1994).
43. T. Kemp, T. A. S. Srinivas, R. Fettig, and W. Ruppel, *Rev. Sci. Instrum*. **66**:176 (1995).
44. G. Langer, J. Hartmann, and M. Reichling, *Rev. Sci. Instrum*. **68**:1510 (1997).
45. M. Reichling and H. Grönbeck, *J. Appl. Phys*. **75**:914 (1994).
46. J. Hartmann, P. Voigt, and M. Reichling, *J. Appl. Phys*. **81**:2966 (1997).
47. M. Bertolotti, G. L. Liakhou, R. Li Voti, S. Paoloni, and C. Sibilia, *J. Appl. Phys*. **83**:966 (1998).
48. H. Shibata, H. Ohta, and Y. Waseda, *JIM Mater. Trans*. **32**:837 (1991).
49. H. S. Carslaw and J. C. Jaeger, *Conduction of Heat in Solids* (Oxford University Press, Oxford, 1959).
50. M. Abramowitz and I. A. Stegun, *Handbook of Mathematical Functions* (Dover, New York, 1970).
51. K. E. Goodson, Ph.D. thesis (Massachusetts Institute of Technology, Cambridge, MA, 1993).
52. M. Nonnenmacher and H. K. Wickramasinghe, *Appl. Phys. Lett*. **61**:168 (1992).
53. M. Maywald, R. J. Pylkki, and L. J. Balk, *Scan. Microsc*. **8**:181 (1994).
54. C. C. Williams and H. K. Wickramasinghe, *Appl. Phys. Lett*. **49**:1587 (1986).
55. K. E. Goodson and M. Asheghi, *Microsc. Therm. Eng*. **1**:225 (1997).
56. G. B. M. Fiege, A. Altes, A. Heiderhoff, and L. J. Balk, *J. Phys. D* **32**:L13 (1999).